Chapter 4

Flow-Enhanced Transient Response in Whispering Gallery Mode Biosensors

4.1 Abstract

Whispering gallery mode (WGM) optical resonator sensors are an extremely sensitive label-free technology for detecting the binding of biomolecules in solution. To better understand the fast transient response observed with these devices, we model mass transfer to spherical and toroidal WGM sensors of identical outer radius. Finite element simulations predict a 3-10 fold higher binding frequency for toroidal sensors. These results agree to within an order of magnitude with experimental data from the literature and suggest a design strategy to improve the transient response of a sensor by making the device small only in the dimension that governs boundary layer development.

4.2 Introduction

Whispering-gallery mode (WGM) optical microcavities [60, 61] are a promising label-free sensing technology that may one day be the basis for high-sensitivity diagnostic and analytical tools capable of detecting biomolecules in complex biological fluids. Recent data demonstrating single-molecule limits of detection [1] have stimulated a debate [97] over the physical processes that enable such a sensitive response when a biomolecule adsorbs to a WGM resonator and interacts with the resonant light. The data published by

Armani and colleagues [1] are extraordinary because of both their sensitivity and the fast response observed, with the latter exceeding the approximate binding rates obtained with mass transfer calculations [98]. The present work examines mass transfer to non-planar, WGM sensors in flow cells, demonstrating how fluid flow and resonator geometry affect the transient sensor response.

The microscale size (i.e., outer diameter $< 100\mu$m) of the WGM sensor, though useful for limiting the amount of sample required, poses a challenge for sample delivery at low concentrations: the overall analyte binding rate is limited by the small surface area. Both the time to achieve a given level of binding during an experiment and the amount of valuable sample required can be reduced by using convection. Some WGM sensor embodiments, like the liquid-core optofluidic ring resonator (OFRR) [99], have their own integrated flow systems. Microfluidic flow cells [30] have also emerged as a popular delivery system due to their small volumes and ease of fabrication, but integration into WGM sensing systems has, understandably, received limited attention in the face of the pressing need for further characterization of basic device performance.

4.3 Boundary Layers

To enable high sensitivity analysis, the flow system must deliver the few analyte molecules in a dilute sample to the sensor as efficiently as possible. The flux of material to the surface of the sensor, $\mathbf{j}_{\text{surf}}$, depends on the concentration gradient evaluated at the surface through Fick's Law, i.e., $\mathbf{j}_{\text{surf}} = -D\nabla c|_{surf}$, where D is the diffusion coefficient. In a quiescent fluid, the gradient scales as $(c|_{surf} - c_\infty)/\ell_s$, where ℓ_s is the characteristic dimension of the sensor. Identifying ℓ_s is obvious for a sphere which has a single dimension, but it is more challenging for the toroid which has two. Flow can limit the extent of the concentration gradient to a thin region of thickness δ at the surface of an object (see Figure 4.1). This so-called *boundary layer* increases the magnitude of the gradient that drives diffusion of the analyte to the sensor and, thereby, enhances the flux.

Squires and colleagues provide an excellent introduction to boundary layer effects in planar sensor performance [98], and develop intuitive relationships between experimental flow parameters and the transient response of those sensors. Their analysis is framed in terms of the Péclet number, a dimensionless group that

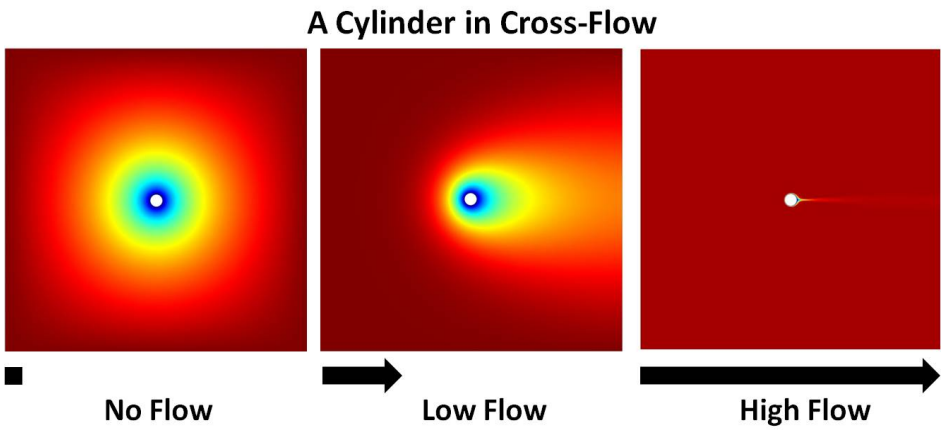

Figure 4.1: Concentration profiles for mass transfer to a cylinder in cross section under various flow conditions. Red denotes a normalized concentration of 1, and Blue denotes a normalized concentration of 0. (a) Diffusion alone delivers the species to the cylinder isotropically. (b) At low upstream flow velocity, an asymmetric concentration distribution forms, with an extended boundary layer in the wake of the cylinder. (c) At high upstream flow velocity, the boundary layer is thin and the concentration gradient remains asymmetric and is confined to a narrow region around the cylinder.

describes the ratio of advective to diffusive timescales, $\mathrm{Pe} = \frac{Ud}{D}$, where U is the inlet flow velocity and d is the critical length scale of the flow obstacle (i.e., sensor diameter). Large values of Pe indicate that advection is dominant and boundary layers are thin. The insights gained in that study provide guidance for understanding the parameters that govern the transient response of non-planar, WGM sensors. The convenient planar, half-sphere, and half-cylinder geometries have been considered elsewhere [100], but ultra-high quality factor WGM sensors and other structures supported on a pedestal have received less attention. For example, these methods are appropriate for nanowire devices [39] that sit on a surface, but they fail to capture the full boundary layer development that occurs for 3-dimensional objects, like the spherical or toroidal sensors, that are removed from the slow-flow region near a substrate.

Mass transport to a small target in flow has been studied extensively in the context of filtration [101], providing a starting point in our effort to analyze flow effects on WGM sensor performance. For our purposes, the biomolecules may be treated as small ($<$ 5 nm diameter) particles undergoing both advection and diffusion. Filtration has traditionally been modeled by considering spheres and cylinders exposed to a uniform upstream flow [101] in an effort to estimate the efficiency with which the filter element will remove

particles from the fluid stream. These studies have established how boundary layers that develop around objects in flow play a critical role in the particle capture process. Convection dominates mass transport far from the object, but the “no slip" boundary condition and the strong adsorption reaction cause both the velocity and the concentration to fall sharply in the boundary layer, where diffusion dominates instead. A typical concentration boundary layer is shown in Fig. 4.2 (inset) for flow around a sphere.

Here we develop a full 3-dimensional model for both spherical and toroidal microresonators using representative dimensions inspired by experimental studies [85, 1]. Specifically, we model a spherical resonator of radius $r_{sphere} = 42.5\,\mu$m and toroidal resonator of major and minor radii $r_a = 40\,\mu$m and $r_i = 2.5\,\mu$m, respectively, so that the two geometries have equal outer radii. In the absence of convenient analytical expressions or approximations like those for the flow fields surrounding spheres and cylinders, the most effective method for solving the momentum balance and continuity equations (i.e., the Navier Stokes equations) for laminar flow around a toroid is to use numerical techniques. Here we use COMSOL Multiphysics, a commercially available finite element (FE) solver, to calculate the velocity and concentration profiles as well as the flux of analyte at the reactor surface. We assume that the fluid is water, and that the inlet has a uniform flow rate (i.e., a flat velocity profile). The concentration of analyte is taken to be 1 fM, and we assume that the system is at steady state. We also assume that the surface binding reaction by the analyte is instantaneous and irreversible, an assumption valid early in the transient measurement when there is insignificant depletion of analyte in the bulk and the vast majority of binding sites on the sensor surface are unoccupied. As a matter of practice, we verified both that the mesh elements used in the FE approximation were sufficiently small to ensure that the mesh size did not impact the accuracy of the calculation (see supplemental information), and that the overall geometry dimensions were large enough that wall effects in the enclosure did not influence the results.

To validate the results of our FE model, we examined the flow around a single spherical resonator of outer radius $r_a = 42.5\,\mu$m. Figure 4.2 shows that these calculations are capable of reproducing the boundary layer depth δ_{95} scaling relationships predicted by Levich [102] and elsewhere [98], where δ_{95} is determined by the distance from the surface of the object at its most upstream point where the concentration reaches

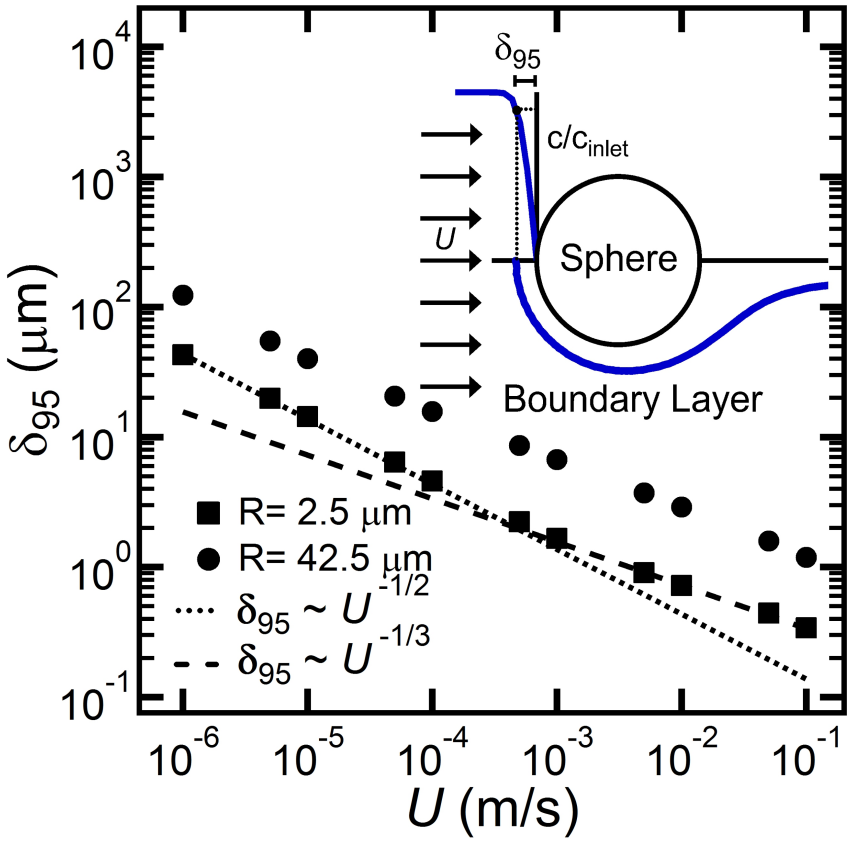

Figure 4.2: Upstream boundary layer thickness δ_{95} as a function of inlet flow velocity for spheres of radius 42.5 μm (circles) and 2.5 μm (squares) with predicted scaling laws at high (blue) and low (red) flow velocity limits. The inset graph depicts how δ_{95} is determined.

95% of the bulk value. Specifically, a small inlet flow velocity, U, yields a boundary layer large compared to the object and that scales with the velocity as $\delta_{95} \sim U^{-\frac{1}{2}}$, but a high inlet flow velocity produces a thinner boundary layer that scales as $\delta_{95} \sim U^{-\frac{1}{3}}$. That these simulations exhibit the predicted asymptotic behavior allows us to proceed with confidence that our model captures the relevant physics.

WGM sensors only yield a signal when biomolecules adsorb where the evanescent field is sufficiently strong, which we take to be $> 10\%$ of the peak mode intensity on the resonator surface. The fraction of this surface where sensing occurs was determined by mode simulations in spherical and toroidal resonators that were performed using the methods presented by Oxborrow [103]. Due to mode compression imposed by the minor radius of the toroid, the effective area for the toroids considered here is $\approx 50\%$ of that for a sphere of

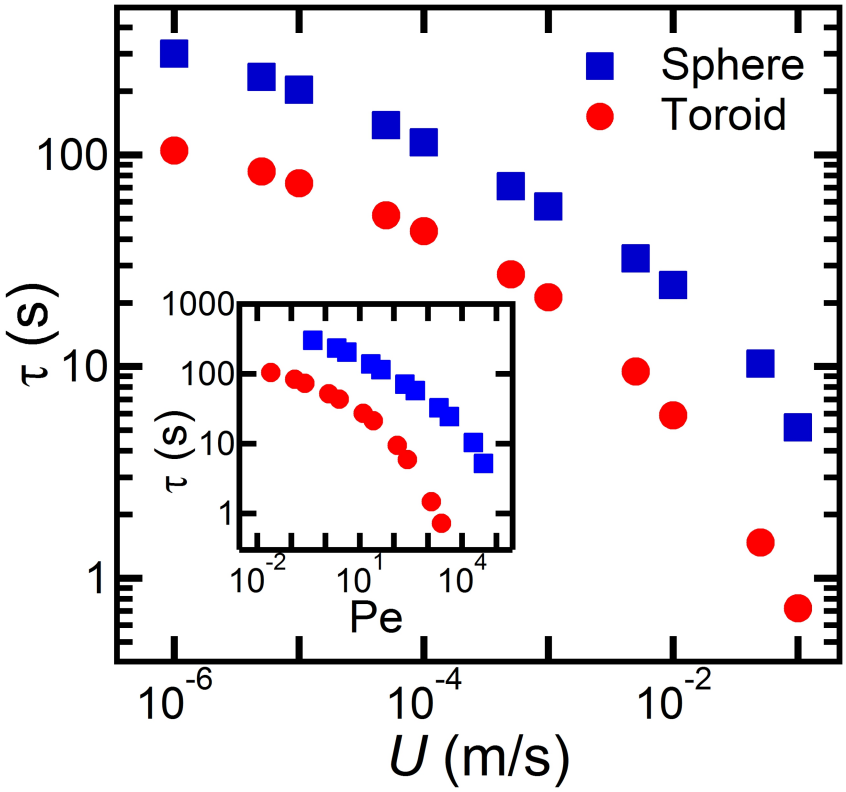

Figure 4.3: Time between binding events, τ, for 1 fM analyte concentration solution introduced to toroidal (circles) and spherical (squares) WGM sensors. (inset) τ recast as a function of sensor Péclet number.

similar major radius (see Section 4.4). We calculate the mean time delay between single-molecule binding events, τ, by integrating the flux over the entire sensing surface and inverting this binding rate.

Despite the somewhat smaller available surface area for interactions with bound material, our model predicts more frequent binding events on a toroidal WGM biosensor than on a spherical one with identical outer radius for all inlet flow velocities studied (Fig. 4.3). The range of accessible flow rates is bounded at low velocity by the ability of most syringe pumps to provide steady, non-pulsatile flow and, at high velocity by the onset of the laminar-turbulent transition regime where the present laminar-flow model is no longer applicable. The different boundary layers that develop around the major and minor diameters of the toroidal resonator lead to consistently shorter response times than those for spheres. In the case of the toroid, the small minor radius thins the boundary layer as did small sphere size in the results shown in

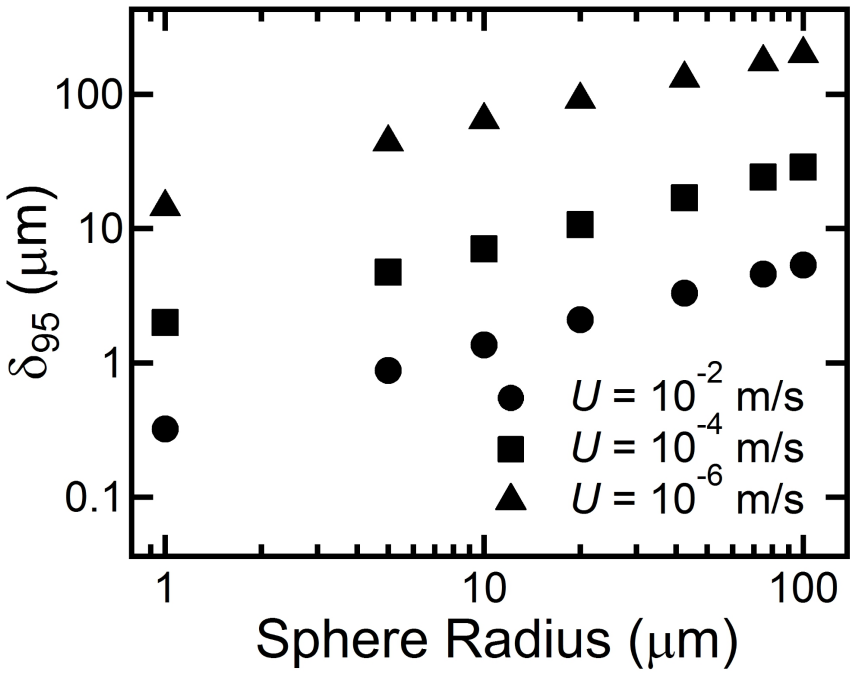

Figure 4.4: The effect of sphere radius on δ_{95} for varying inlet flow velocities, calculated using the same model as in Fig. 4.2.

Fig. 4.4, enhancing the surface flux over that for a sphere with the same outer radius. The toroid experiences a higher binding rate because the increase in analyte flux to the sensor far outweighs the decrease of effective sensing area relative to a sphere.

Toroidal WGM resonators reject many of the non-azimuthal modes that spherical devices exhibit [82]. It is now clear that they offer an additional advantage over spherical sensors because of their enhanced transient response. For inlet flow velocities relevant to the experiments ($U \approx 10^{-2}$m/s) [2], toroids yield 3–10 times more frequent binding events than do spherical devices of similar size. This may explain, at least in part, why single-molecule binding events have been observed only with the former geometry to date.

In Fig. 4.5 we compare the model predictions for τ at various concentrations to single-molecule sensing data gathered with a toroidal WGM sensor by Armani and colleagues [1]. Our simulations of a toroidal device agree with these experimental data to within an order of magnitude, while those for a spherical sensor poorly describe these data (inset). Refinement of the computational model may further reduce these discrepancies. In particular, we leave for future work the incorporation of the chip from which the toroids

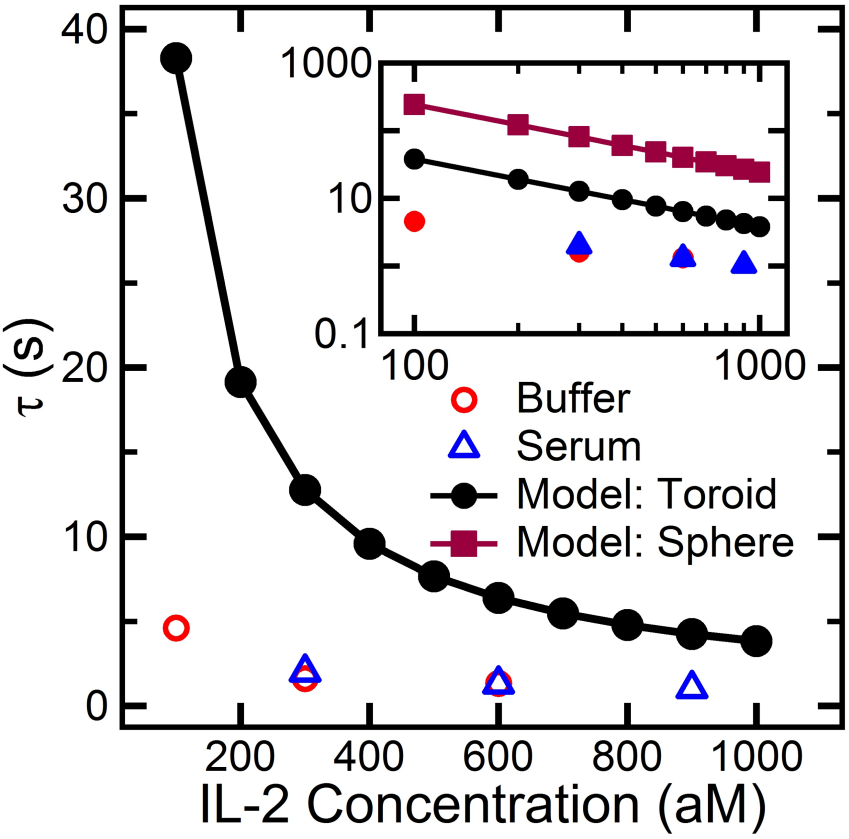

Figure 4.5: Modeled results for τ at a range of concentrations for Interleukin-2 with $U = 10^{-2}$ compared to experimental data published by Armani et al. [1, 2] collected in buffer (circle) and bovine blood serum (triangle).

are fabricated into the simulated geometry as well as a consideration of equilibrium binding of analyte to the functionalized device.

This study uses a finite element computational model to investigate mass transfer to spherical and toroidal WGM optical biosensors in flow. The thickness of boundary layers that develop around these devices determine the flux of analyte to the surface and, consequently, the transient signal of the sensor. Our simulations show that the minor diameter of a toroidal device produces a thinner boundary layer than for a sphere of identical outer radius, allowing the toroid to experience more frequent binding events. These results support experimental observation in the literature [1] and illuminate a strategy that may be broadly applied to sensor design that will result in a more rapid transient device response. Making the sensor small

only in the dimension that governs boundary layer development simultaneously maximizes both surface flux of analyte and the effective sensing area of the device.

This work was supported by funding from the Jacobs Institute for Molecular Engineering for Medicine at the California Institute of Technology.

4.4 Supplemental Information

Numerical Solutions

Calculating the rate at which a species reaches the sensor surface involves solving the momentum and continuity differential equations to describe fluid flow (e.g., the Navier-Stokes equations) as well as solving the conservation of mass equation, which requires knowledge of the flow velocity field. For a single species with concentration, C_i, in an incompressible Newtonian fluid, these equations are expressed as

$$\rho\Big(\frac{\partial \mathbf{u}}{\partial t} + \mathbf{u}\cdot\nabla\mathbf{u}\Big) = -\nabla p + \mu\nabla^2\mathbf{u} \tag{4.1}$$

$$\nabla\cdot\mathbf{u} = 0 \tag{4.2}$$

$$\frac{\partial C_i}{\partial t} + C_i\nabla\mathbf{u} = D\nabla^2 C_i \tag{4.3}$$

where ρ is the fluid density, $\mathbf{u}$ is the velocity, p is the pressure, μ is the viscosity, and D is the diffusion coefficient.

We use a commercially available finite element (FE) solver, COMSOL Multiphysics 4.1, to solve this system of equations on a server with 32 64-bit AMD processors and 256 GB DDR-2 RAM. The FE method involves breaking the geometry over which the equations apply (i.e., the "flow cell") into small tetrahedral volumes and applying boundary conditions at each face of an element. This powerful method allows the user to focus computation power on parts of the geometry where the solution varies most strongly with position by locally controlling element size. Elements at the edge of the volume experience the macro-scale

boundary conditions commonly imposed when solving differential equations analytically, while those in the interior experience a “continuity boundary condition" that applies to the dependent variables as well as their derivatives.

Figure 5.7 shows the flow cell used for the present work, comprising a rectangular flow cell with a symmetry plane that bisects both the cell as well as the sensor. This half cell is 2.5 mm in the flow direction, and 1.5 mm x 1.5 mm in cross section (3 mm wide by 1.5 mm tall for the full cell). These dimensions were determined to be sufficiently large that increasing them led to less than 1% change in integrated analyte adsorption rates to the sensor for all flow rates considered here.

The sensor surface features a “no-slip" boundary condition typical of solid walls and the analyte is assumed to adsorb instantaneously there. Figure 4.7 shows additional boundary conditions. We assume a flat profile for the inlet flow velocity, U_{inlet}, and an inlet analyte concentration of $C_{inlet} = 1$ fM. The top, bottom, and side boundaries are given “no-slip" and “no flux" conditions, while the flow outlet is set to atmospheric pressure $p_0 = 101{,}325$ Pa. The diffusion coefficient of Interleukin-2 (IL2, Mw 15.5 kDa) was approximated to be$D \approx 10^{-10}\mathrm{m}^2/\mathrm{s}$ [104].

The array of elements used in an FE solver is called the *mesh*, and its design can significantly impact the accuracy of the mathematical solution. A balance must be struck between making the mesh elements small enough to capture local changes in dependent variables and making them prohibitively small that the computer has insufficient resources to find a solution. We evaluate the dependence of our results on surface mesh element size, l_{mesh}, by studying flow around a spherical sensor of radius $R_{sphere} = 42.5\,\mu$m and $U_{inlet} = 0.01$ m/s. We set l_{mesh} to be a maximum of R_{sphere}/N and calculate the steady-state binding rate to the entire sensor surface. These data are reported in Fig. 4.8 as a relative binding rate with respect to that calculated for the case $N = 500$ where

$$\Phi_{N=500} = \frac{\mathrm{Bindingrate for} N}{\mathrm{Bindingrate for} N = 500}. \tag{4.4}$$

This limiting condition ($N = 500$) represents the mesh size beyond which solutions take prohibitively long

to converge. The value of $\Phi_{N=500}$ is greater than 0.98 for N $>$ 80, indicating an acceptable 2% relative error. Therefore, we set the surface mesh size in all models for the current work as 1/80 of the critical dimension (R_{sphere} for a sphere and r_{minor} for a toroid).

While analyte is assumed to adsorb to the entire surface of the resonator, only a fraction of that surface is effective for sensing. COMSOL solutions for the mode in a spherical and toroidal WGM resonator, calculated using methods described by Oxborrow [103], were used to identify the functional region of the sensor defined by where the mode intensity at the resonator surface is >10% of the surface maximum. These results are shown in Fig. 4.9. The effective mode height for the toroid modeled here ($h_{mode} = 2.84\,\mu$m) is less than half that for a sphere of identical outer radius ($h_{mode} = 6.00\,\mu$m) due to mode compression by the minor radius of the toroid.

Single-Molecule Binding Data

We compare the predictions of our model with single-molecule binding data observed experimentally by Armani and colleagues [1]. Those data are transient measurements monitoring the resonant wavelength, λ_R , of the mode as interleukin-2 binds to the resonator, which has been functionalized with anti-IL2. The sensor exhibits a step-wise response in λ_R for a range of IL2 concentrations regardless of whether buffer or bovine blood serum was used as the solvent. The experimental data included in Fig. 4.5 represents the average time between binding events detected during the first 60 seconds of the experiment. This time window was chosen in accordance with the assumptions made in the computational model. A step was defined as any time $|\Delta\lambda_R| > 2\sigma$, where σ is the noise of the signal in λ_R within a single step and averaged over the first five steps in an experiment. Typical values of σ were between 0.15 fm (0.15$\times$ 10-15 M) and 0.25 fm.

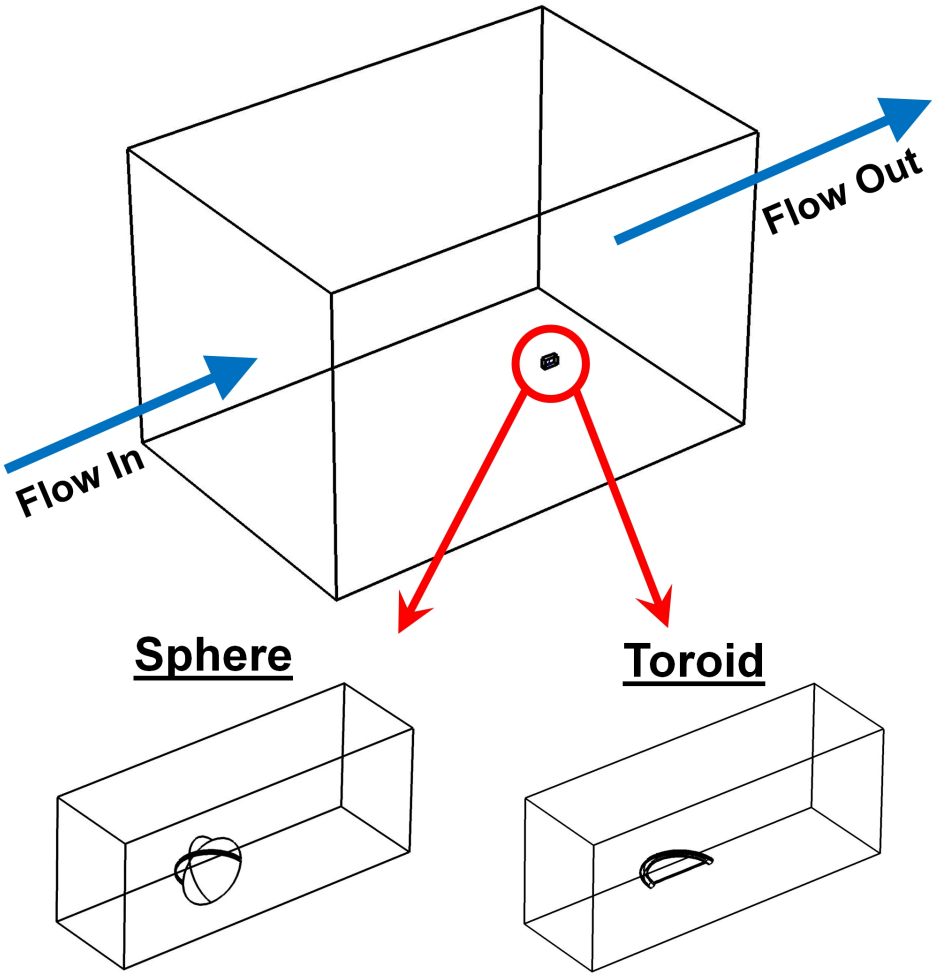

Figure 4.6: Flow cell geometry used in COMSOL Multiphysics simulation of flow around a WGM sensor. The near plane is a symmetry plane that bisects the cell and the resonator. The sensors are cut out of the cell, and their surfaces feature no-slip flow and $C_i = 0$ (i.e., instantaneous surface reaction) boundary conditions.

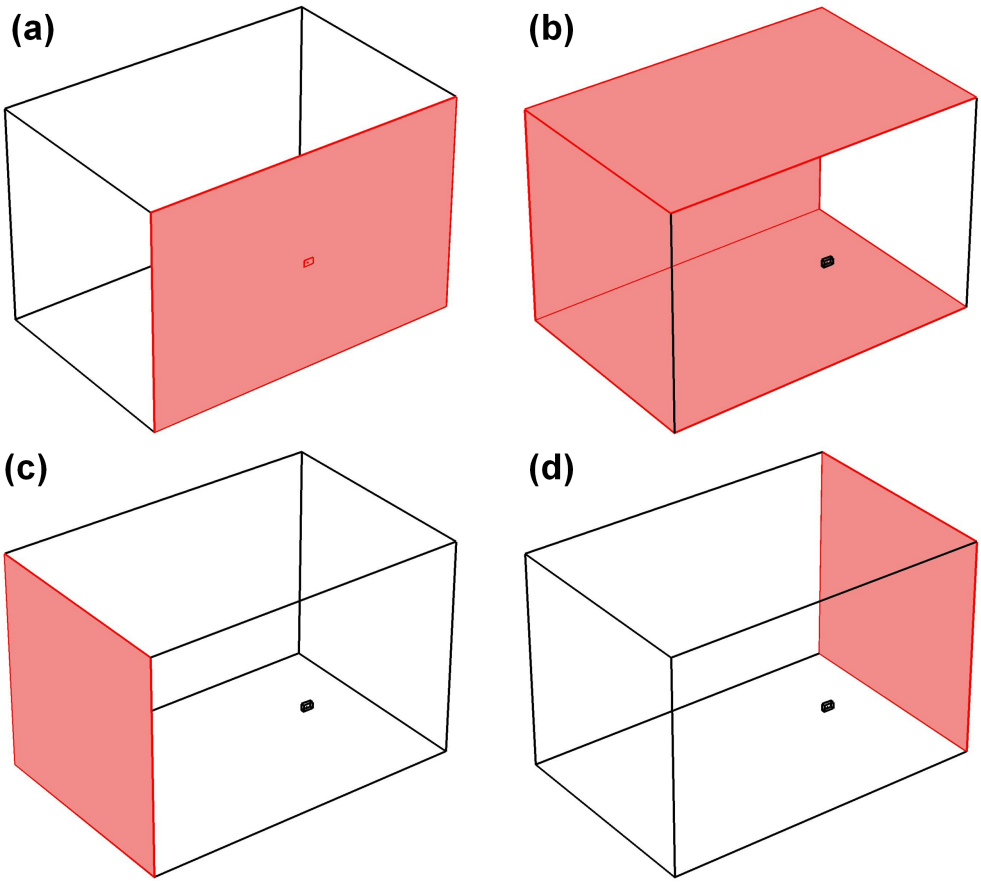

Figure 4.7: Flow cell boundary conditions used in COMSOL Multiphysics simulations of flow around WGM sensors. (a) Symmetry plane. (b) “No-slip" and “no flux" conditions. (c) Uniform flow inlet velocity $U = U_{inlet}$ and inlet concentration $C_{inlet} = 1$ fM. (d) Flow outlet at pressure $p_0 = 101{,}325$ Pa.

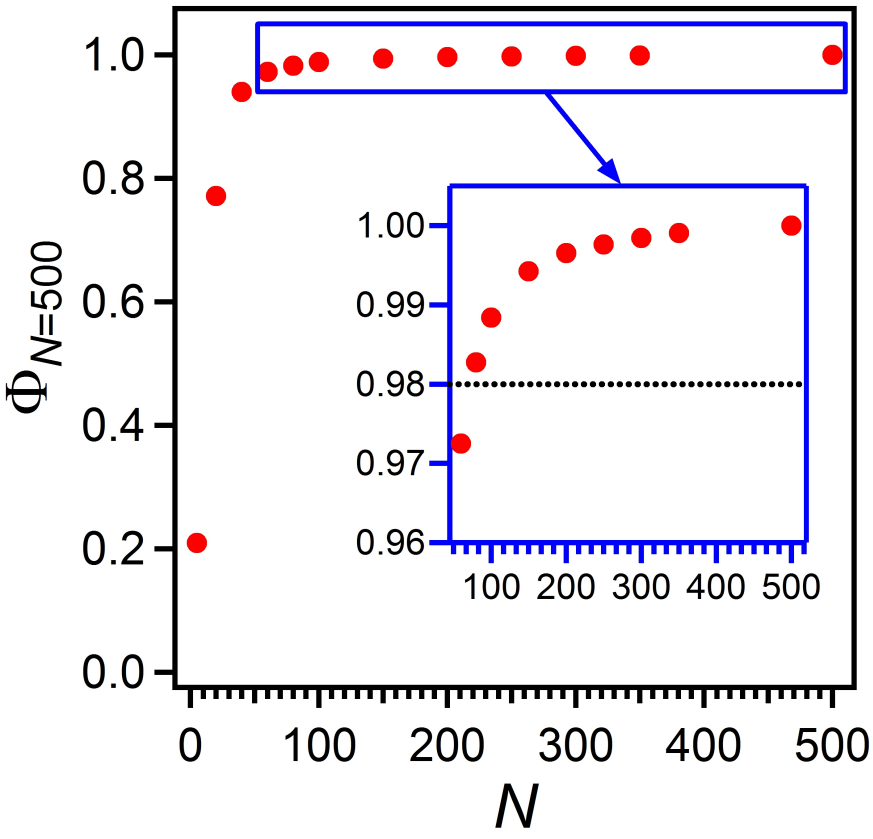

Figure 4.8: The relative surface binding rate to a sphere with $R_{sphere} = 42.5\,\mu m$ and $U_{inlet} = 0.01$ m/s as a function of the surface mesh element size ($l_{mesh} = R_{sphere}/N$), calculated with respect to the case $N = 500$ ($l_{mesh} = 85$ nm). This quantity converges with increasing N and achieves a relative error of less than 2% for N $>$ 80 (see inset for detail).

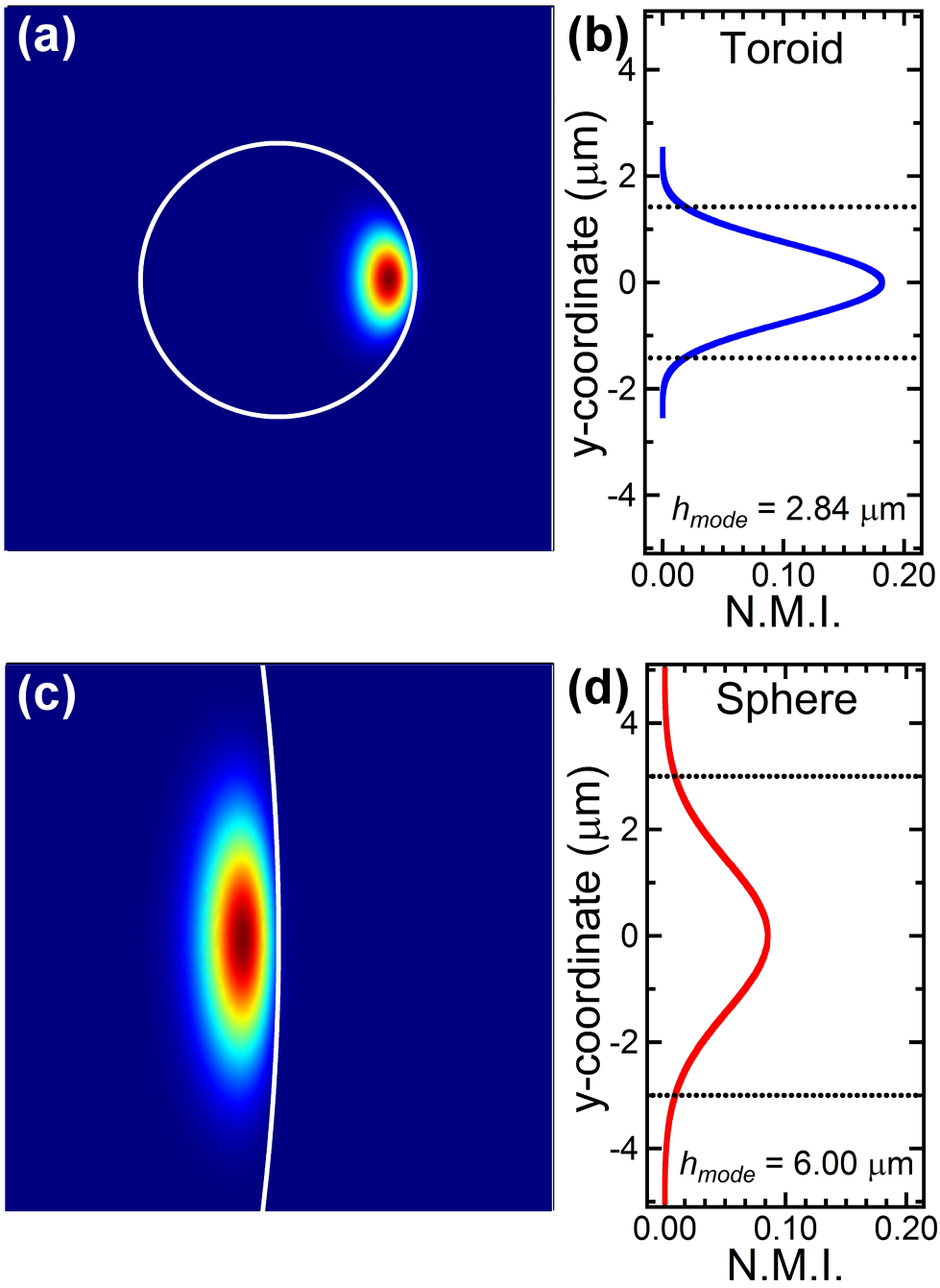

Figure 4.9: Solutions for the normalized mode intensity (NMI) of a (a) toroidal and (c) spherical optical whispering gallery mode resonator. The effective sensing area is determined by where the NMI is greater than 10% of the surface maximum as indicated by dotted lines for (b) a toroid and (d) a sphere.